# Stress Changes the Material State of a Bacterial Biomolecular Condensate and Shifts its Function from mRNA Decay to Storage

Luis A. Ortiz-Rodríguez[1], Hadi Yassine[2,3], Ali Hatami[4], Vidhyadhar Nandana[2], Christopher A. Azaldegui[5], Jiayu Cheng[1], Yingxi Zhu[4], Jared M. Schrader[2,3*], Julie S. Biteen[1,5*]

[1]Department of Chemistry, University of Michigan, Ann Arbor, MI 48109 USA.

[2]Departments of Chemistry and Biological Sciences, Wayne State University, Detroit, MI 48202 USA.

[3]Department of Biology, Indiana University, Bloomington, IN 47405 USA.

[4]Department of Chemical Engineering and Materials Science, Wayne State University, Detroit, MI 48202 USA.

[5]Doctoral Program in Chemical Biology, University of Michigan, Ann Arbor, MI 48109, USA.

[*]To whom correspondence should be addressed: jsbiteen@umich.edu, jaschrad@iu.edu

## Abstract

Bacterial ribonucleoprotein bodies (BR-bodies) are dynamic biomolecular condensates that play a pivotal role in RNA metabolism. We investigated how BR-bodies significantly influence mRNA fate by transitioning between liquid- and solid-like states in response to stress. With a combination of single-molecule and bulk fluorescence microscopy, biochemical assays, and quantitative analyses, we determine that BR-bodies promote efficient mRNA decay in a liquid-like condensate during exponential growth. On the other hand, BR-bodies are repurposed from sites of mRNA decay to reservoirs for mRNA storage under stress; a functional change that is enabled by their transition to a more rigid state, marked by reduced internal dynamics, increased molecular density, and prolonged residence time of ribonuclease E. Furthermore, we manipulated ATP levels and translation rates, and we conclude that the accumulation of ribosome-depleted mRNA is a key factor driving BR-body rigification, and that condensate maturation further contributes to this process. Upon nutrient replenishment, stationary-phase BR-bodies disassemble, releasing stored mRNAs for rapid translation, demonstrating that BR-body function is governed by a reversible mechanism for resource management. These findings reveal adaptive strategies by which bacteria regulate RNA metabolism through condensate-mediated control of mRNA decay and storage.

## Introduction

Biomolecular condensates are dynamic macromolecular assemblies that often form via phase separation,[1,2] a reversible process that enables the cell to respond rapidly to environmental changes.[3] These assemblies are selectively permeable and can exchange client molecules.[1,4] Depending on their physical state, which can range from liquid droplets to hydrogels and insoluble aggregates, condensates facilitate various biological functions.[1,5] Liquid-like condensates promote biochemical reactions by allowing internal

35 diffusion and exchange with the dilute phase, while gel- and solid-like condensates have reduced diffusion
36 and exchange, which slow down biochemical reactions and may potentially sequester biomolecules for
37 storage.[1,2] Notably, transitions from the liquid to solid state in biomolecular condensates have been linked
38 to neurodegenerative protein aggregation disorders:[6,7] reducing the fluidity of these condensates can
39 negatively affect their function.[8,9] However, in other cases, such as germ granules, solid-like states play
40 important roles in mRNA storage and translational control in the developing embryo.[10]

41 Recently, biomolecular condensates have emerged as a broadly utilized mechanism for organizing
42 diverse biochemical pathways within the bacterial cytoplasm,[11–19] and this organizational paradigm is
43 particularly important in bacteria because these organisms generally lack membrane-bound organelles.[20,21]
44 Bacterial ribonucleoprotein bodies (BR-bodies), the organelles that contain the RNA degradation machinery,
45 were the first bacterial condensates demonstrated to assemble via liquid-liquid phase separation (LLPS),
46 driven by interactions between the large intrinsically disordered region (IDR) of ribonuclease E (RNE; Fig. 1a)
47 and RNA.[11]

48 *Caulobacter crescentus* BR-bodies share functional similarities with eukaryotic processing bodies
49 (P-bodies) and stress granules (SGs), as all three contain the mRNA decay machinery. RNE (Fig. 1a), the
50 core scaffold and driver of BR-body function, is the essential and rate-limiting factor in bacterial mRNA
51 decay.[22,23] Similarly, Xrn1 is a core component of eukaryotic P-bodies and SGs, and it controls cytoplasmic
52 mRNA decay.[24–26] In addition, similar types of molecules are enriched in BR-bodies (Fig. 1b,c), P-bodies, and
53 SGs, including DEAD-box RNA helicases, Lsm proteins, miRNAs, small-RNAs, and translationally repressed
54 mRNAs.[27] P-bodies and SGs have been predominantly studied under conditions of cell stress, and some
55 studies indicate that P-bodies promote mRNA decay, while others show an mRNA storage function,
56 whereas SGs have only been found to promote storage.[11,25,28] These differences in the decay and storage
57 functions are correlated with differences in the mobility of molecules within P-bodies[25,28–31] and SGs,[32–34]
58 since P-bodies have been found to have higher mobility and more rapid exchange with the dilute phase than

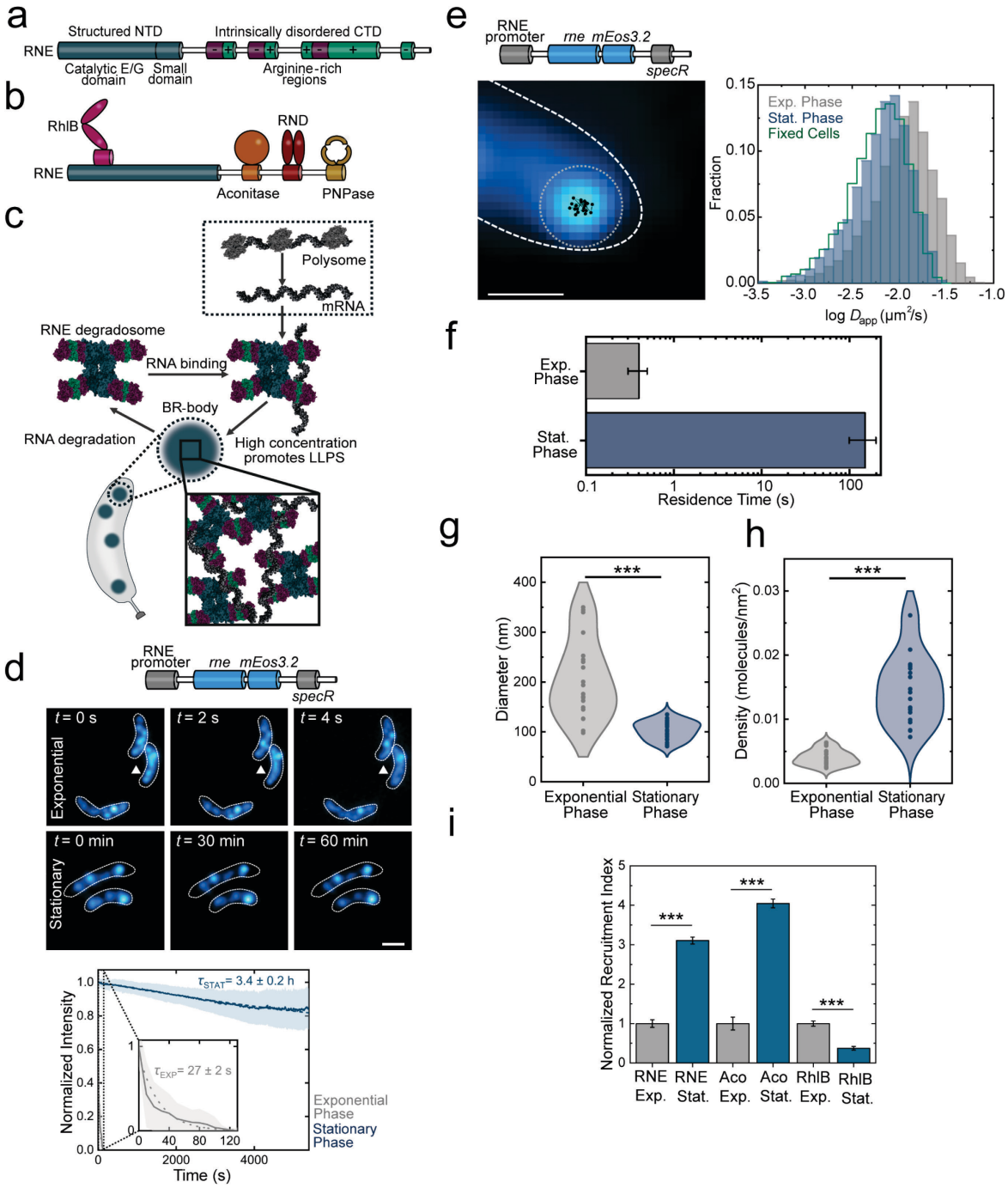


**Fig. 1 | BR-bodies are dynamically arrested and compacted upon entering stationary phase.**

**Fig. 1 | BR-bodies are dynamically arrested and compacted upon entering stationary phase**. (a) Domain organization of *C. crescentus* RNase E (RNE). (b) The *C. crescentus* RNA degradosome includes RNE, RhlB, aconitase, RNase D, and PNPase. The RNE NTD has an RhlB binding site. The CTD has interaction sites for aconitase, RNase D, and PNPase. (c) In the working model for BR-body-mediated mRNA decay, untranslated mRNAs and the RNE degradosome can phase separate into a biomolecular condensate, thereby increasing their local concentration and accelerating decay processes within the BR-body. The condensate dissolves as mRNA is degraded, releasing degradosome components and oligonucleotides. (d) Lifespans of condensates based on an RNE-mEos3.2 construct (top). Middle: representative images of *C. crescentus* cells (white outlines) and RNE-mEos3.2 (blue) in each phase as a function of imaging time, *t*; arrowheads indicate representative RNE-mEos3.2 foci. Scale bar: 500 nm. Bottom: decay profiles of photobleaching-corrected intensities with estimates of the average condensate lifespans, $\tau_{EXP}$ and $\tau_{STAT}$, in exponential and stationary phases, respectively. Analyses include $N$ = 427 foci in 211 cells (exponential) and $N$ = 932 foci in 232 cells (stationary). (e-i) Dynamics of degradosome components within BR-bodies across growth phases. (e) Single-molecule tracking of RNE inside BR-bodies. Top-left: genetic construct used to track RNE. Bottom-left: a representative single-molecule trajectory of RNE-mEos3.2 within a BR-body (dotted circle) in a *C. cresentus* cell (dashed lines). The black dots indicate the super-localized positions of the molecule in consecutive 20-ms imaging frames. Scale bar: 500 nm. Right: Changes in the diffusivity of RNE within BR-bodies across growth phases. Number of trajectories analyzed: 5,001 (exponential phase) and 6,347 (stationary phase). The apparent diffusion coefficients for RNE-mEos3.2 trajectories in live cells are compared to the apparent diffusion coefficients of trajectories in fixed cells to distinguish between diffusing and static molecules. (f) Increase in residence time of RNE-mEos3.2 of BR-bodies between exponential and stationary phase. (g) Increase in BR-body diameter between exponential and stationary phases. The BR-body diameter is estimated as the maximum span of the cluster identified using density-based cluster analysis. Number of clusters analyzed: 20 per condition. (h) Increase in the density of RNE-mEos3.2 single-molecule localizations within BR-bodies during the transition from exponential to stationary phase. Each point shows the density in one condensate. Number of clusters analyzed: 20 per condition. (i) Normalized recruitment index of degradosome components RhlB-PAmChy, Aco-PAmChy, and RNE-mEos3.2 inside the BR-bodies in stationary phase relative to the recruitment in exponential phase, indicating the presence of incomplete degradosomes in BR-bodies during stationary phase. Error bars represent propagated standard deviations. All NRI values were normalized to the mean NRI of the exponential phase, setting the exponential phase values to 1. The error for each condition was calculated by propagating the original standard deviation using standard error propagation rules. Error bars in f and i: standard deviation from three biological replicates. *** in g and i denotes $p < 0.001$.

59 SGs. BR-bodies have been predominantly studied in exponentially growing bacteria cells, during which they
60 appear to have liquid-like properties that promote mRNA decay (Fig. 1c).[11,35] In contrast, under cell stress,
61 BR-bodies undergo increased condensation that correlates with enhanced survival under these conditions,
62 yet their internal dynamics and rates of mRNA degradation have not been previously explored under stress.[11]
63 Evidence from multiple bacterial species has shown that mRNA decay rates are reduced under conditions
64 of nutrient limitation, such as when cells enter stationary phase, yet the role of BR-bodies in this slowdown
65 of mRNA decay has not yet been explored.[36–41]

66 In this study, we investigate changes in the dynamics within BR-bodies between exponential growth
67 and stationary phase and how these differences impact the mRNA decay pathway. We define the material
68 state of a biomolecular condensate as the set of physical properties that determine internal mobility,
69 exchange with the surrounding environment, condensate compaction, and thus biological function.
70 Furthermore, in this work, a condensate is considered liquid-like when it exhibits dynamic internal
71 rearrangement, rapid molecular exchange with the surrounding environment, lower biomolecular density,
72 and short residence times of key components, while rigid condensates show reduced internal molecular
73 diffusion, longer component residence times, increased compaction, and reduced exchange with the
74 surrounding environment. Our live-cell single-molecule microscopy results demonstrate that BR-bodies
75 transition from a dynamic, liquid-like state during exponential growth to a less dynamic, more rigid material
76 state during stress. We demonstrate that this transition is associated with a functional shift from enhancing
77 mRNA decay in exponential phase to promoting mRNA storage in the rigid state. In line with these results,
78 we measure that the *in vitro* maturation of RNE condensates and subsequent arrest of dynamics lead to a
79 strong reduction in RNE activity. Given the similarities between BR-bodies and eukaryotic biomolecular
80 condensates like SGs and P-bodies, our findings further suggest that differences in cell growth conditions
81 may also alter the material properties of P-bodies and SGs to shift the inherent preferences for mRNA decay
82 vs. storage across diverse organisms.

83 **The transition from exponential to stationary phase is associated with BR-body rigidification**

84 To investigate the dynamics of molecules within BR-bodies and their response to stress, we labeled
85 the endogenous copy of RNE with the green-to-red photoconvertible fluorescent protein mEos3.2 (RNE-
86 mEos3.2; Fig. 1d).[42] This labeling strategy allows us to study the properties of BR-bodies as a whole using
87 bulk fluorescence in the initial mEos3.2 green state, and to measure their internal dynamics at the single-
88 molecule level in the mEos3.2 red state after photoconversion using 405-nm excitation. We compared BR-
89 body dynamics during exponential and stationary growth phases to understand the effect of non-invasively
90 induced cellular starvation, ensuring physiologically relevant observations of the stress response. We
91 further sought to resolve two previous confounding observations: (1) there is an increased number of BR-
92 bodies and a higher copy number of RNE in each condensate in cells at stationary phase (Extended Data
93 Fig. 1a and Supplementary Figure 1),[11] a nutrient-deprived state during which bacterial growth and division
94 cease, and yet (2) mRNA decay is slower in stationary phase.

95 To investigate how stationary phase alters BR-bodies, we performed time-lapse imaging of cells in
96 exponential and stationary phases. In exponential phase, BR-bodies rapidly assemble and disassemble,
97 consistent with their known role in mRNA decay (Fig. 1d, Supplementary Movie 1). However, in stationary
98 phase, BR-bodies are dramatically stabilized (450-fold; Fig. 1d, Supplementary Movie 2). As RNA is required
99 for BR-body phase separation,[11] the decreased dissolution rate of BR-bodies during stationary phase
100 suggests reduced RNA decay activity, as mRNA degradation is necessary for BR-body disassembly (Fig.
101 1c).[11] Single-molecule tracking of RNE-mEos3.2 and the degradosome protein aconitase-PAmChy,
102 previously identified as a direct binding partner to RNE[11,43,44] and core component of the *C. crescentus* RNA
103 degradosome, revealed measurably reduced diffusivity of RNE and its degradosome client proteins within
104 BR-bodies during stationary phase (Fig. 1e and Extended Data Fig. 1b, c), consistent with a more rigid
105 internal microenvironment. In addition, we compared RNE-mEos3.2 diffusion in both growth phases with
106 the apparent diffusion of immobile RNE-mEos3.2 molecules in fixed cells. While we measured slow

107 diffusion of RNE-mEos3.2 within BR-bodies during exponential phase, this value is higher than our lower
108 bound as determined in fixed cells. In contrast, the diffusion profile of RNE-mEos3.2 in stationary phase
109 cells closely matches that of fixed cells, suggesting that, under our experimental conditions, RNE-mEos3.2
110 is essentially static within the BR-bodies during stationary phase. Furthermore, the residence time of RNE
111 within BR-bodies is 370-fold longer in stationary phase compared to exponential phase (Fig. 1f). After
112 identifying the RNE-mEos3.2 clusters with a density-based cluster analysis,[45] we determined the molecular
113 density and estimated the BR-body diameter, $\bar{d}$, as the maximum span of each cluster (Fig. 1g,h). In
114 exponential phase, the BR-bodies are less dense and larger ($\bar{d}$ = 206 ± 2 nm) than in stationary phase ($\bar{d}$ =
115 102 ± 1 nm) (mean ± SEM; $p < 0.001$). Importantly, the decreased diffusivity and increased residence time
116 of RNE within the BR-bodies, along with their compaction, are also observed under ethanol stress, indicating
117 that dynamic arrest behavior likely occurs under other inducing stresses (Extended Data Figs. 1d–f,2). This
118 compaction explains the decreased internal dynamics, where the rigid state constrains RNE within the BR-
119 body.

120 We also analyzed the diffusion of RNE outside the BR-bodies in both exponential and stationary
121 phase cells to determine whether the observed changes in RNE mobility were specific to the condensate
122 internal microenvironment. The mobility of RNE molecules not associated with the BR-bodies remained
123 unchanged between growth phases (Extended Data Fig. 1c), indicating that the reduced mobility observed
124 within BR-bodies during stationary phases arises from changes in the condensate internal
125 microenvironment rather than reflecting overall cellular changes between growth phases. This lack of a
126 change in diffusion outside the BR-bodies reflects the short timescales probed by our single-molecule
127 trajectories (~160 ms), which primarily report on local motions and therefore do not capture slower
128 cytoplasmic dynamics.[46] In contrast, the microenvironment within stationary phase BR-bodies is
129 sufficiently dense that a measurable reduction in RNE-mEos3.2 mobility is evident even on these short

130 timescales, while condensate-level diffusion becomes distinct at longer observation windows
131 (Supplementary Figure 2).

132 To determine whether BR-bodies retain characteristics of phase-separated condensates during
133 stationary phase, rather than forming irreversible aggregates, we treated cells with 5% 1,6-hexanediol (HD),
134 a commonly used aliphatic alcohol that disrupts the weak hydrophobic interactions essential for phase
135 separation.[47–49] BR-bodies dissolve within ~ 25 minutes of HD treatment (Extended Data Fig. 1g), confirming
136 that they remain sensitive to HD despite rigidification during stationary phase. This finding suggests that BR-
137 bodies retain hallmark features of biomolecular condensates, even in the rigid state, and that the observed
138 rigidification reflects a dynamic arrest rather than a transition to an aggregated or misfolded state.

139 BR-bodies concentrate the RNA degradosome complex, which in *C. crescentus* contains aconitase,
140 RhlB, and PNPase (Fig. 1b).[11,44] We quantified the recruitment of aconitase and RhlB to BR-bodies during
141 exponential and stationary phases, normalizing by differences in overall expression levels. After
142 normalization, we found that aconitase recruitment increases 4-fold, while RhlB recruitment decreases 3-
143 fold in stationary phase (Fig. 1i). These results reveal a stoichiometric reorganization of BR-bodies under
144 stress. In particular, the concomitant loss of RhlB and enrichment of RNE and aconitase indicate the
145 presence of incomplete degradosomes inside BR-bodies during stationary phase. DEAD-box RNA helicases
146 are central regulators of biomolecular condensates;[50] their ATPase cycle maintains the condensates in a
147 dynamic, non-equilibrium state, facilitating the enrichment of client molecules and buffering the dispersed
148 ribonucleoprotein pool. The decreased recruitment of the DEAD-box RNA helicase RhlB thus likely impairs
149 the internal remodeling of BR-bodies, potentially contributing to their rigidification during stress.

150 **Increased levels of poorly translated mRNA and maturation trigger the transition to the rigid**
151 **material state**

152 During stationary phase, bacterial cells encounter nutrient scarcity, which slows down
153 cellular processes including metabolic activity, leading to lower ATP levels (Fig. 2a).[51] Reduced ATP
154 levels subsequently impact various processes, including protein synthesis and translation, promote
155 phase separation of proteins with intrinsically disordered regions (IDRs),[18] contribute to protein
156 aggregation,[12,13] and cause physical changes in cytoplasm,[46,52] creating a glassy state that slows the
157 diffusion of mesoscale objects such as BR-bodies (Supplementary Figure 2). Additionally, since
158 DEAD-box helicases like RhlB require ATP hydrolysis to remodel, dissolve, cooperatively bind RNA,[53]
159 prevent strong interactions, and maintain the fluidity of the condensates,[50] the low ATP levels at
160 stationary phase may impair these activities.

161 To separate the effects of low ATP levels and reduced translation on BR-body rigidification,
162 we artificially decreased ATP and translation levels in exponential phase cultures of *C. crescentus*.
163 To lower ATP levels, we treated the cultures with the protonophore carbonyl cyanide *m*-chlorophenyl
164 hydrazone (CCCP) to disrupt the proton motive force,[54] rapidly inhibiting ATP synthase. A 20-min
165 treatment with 100 μM CCCP was found to reduce cellular ATP concentrations to levels comparable
166 to those observed during stationary phase (Fig. 2a). To reduce translation levels, we used puromycin
167 (150 μg/mL for 30 min), which prematurely cleaves peptide chains[55] and releases ribosome subunits
168 and mRNA, thereby increasing the availability of ribosome-depleted transcripts in the cytoplasm.
169 Since puromycin treatment also results in ATP levels similar to those observed in stationary phase
170 (Fig. 2a), we treated cells with CCCP and the translation elongation inhibitor chloramphenicol as a
171 control. Chloramphenicol prevents translation by blocking peptide bond formation and
172 accumulating ribosomes on mRNA.[56] Interestingly, treating exponential phase cultures with CCCP
173 and puromycin leads to long-lived BR-bodies (Fig. 2b), similar to those observed during stationary

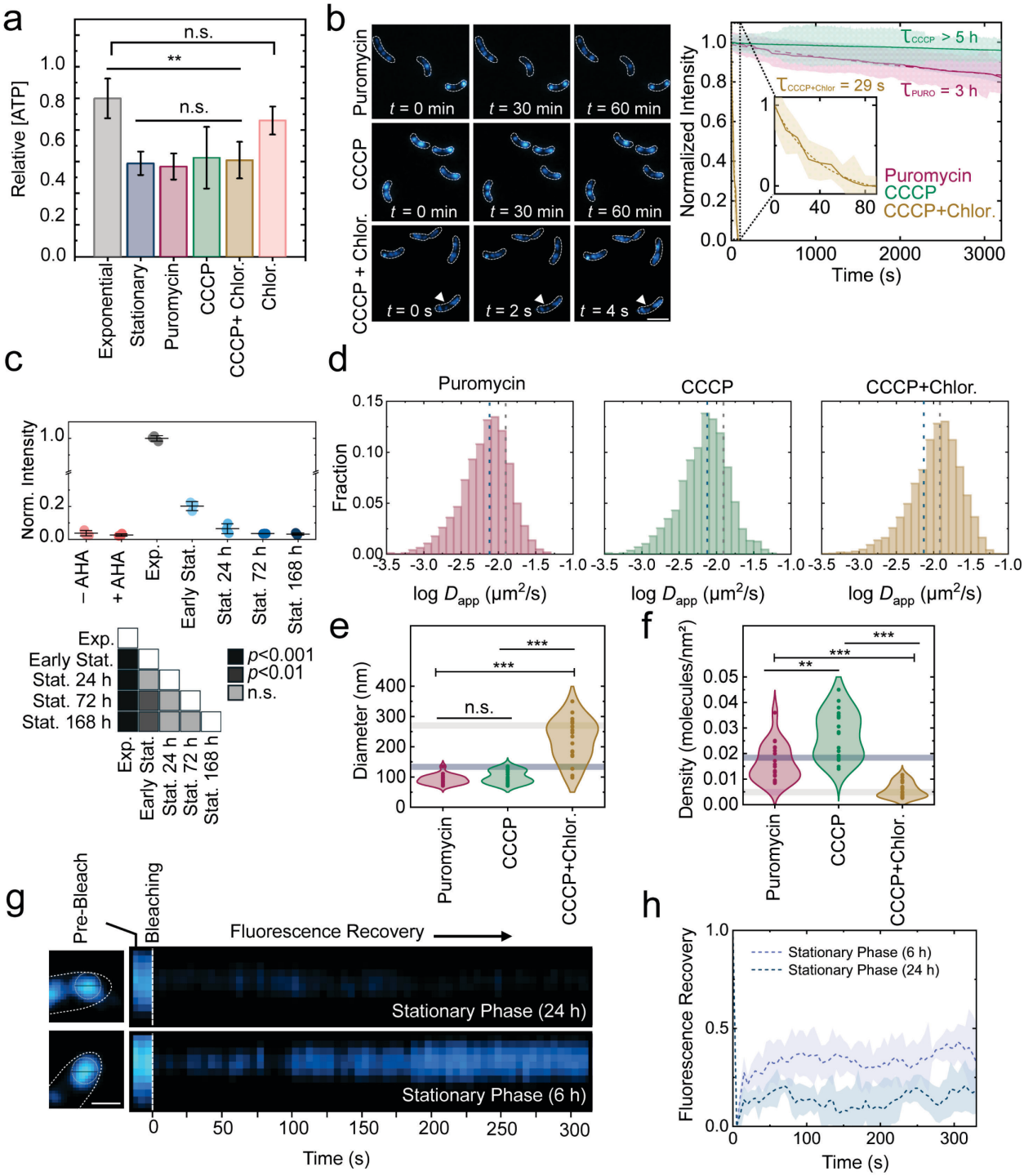


**Fig. 2 | Rigidification of BR-bodies is promoted by increased levels of poorly translated mRNAs.**

**Fig. 2 | Rigidification of BR-bodies is promoted by increased levels of poorly translated mRNAs**. (a) Quantification of intracellular ATP concentrations in *C. crescentus* using a luciferase-based assay following no treatment or treatment as described. ATP levels are normalized to exponential growth levels. (b) Lifespans of BR-bodies in cells under the acute treatment conditions described in (a). Left: Representative images of RNE-mEos3.2 (blue) in *C. crescentus* cells (white outlines) as a function of treatment and imaging time, *t*. Arrowheads indicate representative RNE-mEos3.2 foci. Scale bar: 2 μm. Right: Decay profiles of photobleaching-corrected intensities used to estimate the average condensate lifespan. Analyses include $N$ = 308, 347, and 241 foci for puromycin, CCCP, and CCCP + chloramphenicol, respectively, measured across 88, 193, and 301 cells, respectively. (c) Top: relative translational levels in exponential and stationary phases using Biorthogonal Non-Canonical Amino Acid Tagging (BONCAT), and controls with azidohomoalanine (AHA) and chloramphenicol and without AHA. Error bars: standard deviation of three replicates. Bottom: statistical analysis. (d) Impact of acute treatments on the diffusivity of the BR-body RNE scaffold. The distribution of apparent diffusion coefficients for RNE-mEos3.2 trajectories is measured following each treatment. Vertical dashed lines: distribution medians. Number of trajectories analyzed: 2,126 (puromycin), 1,637 (CCCP), and 1,441 (CCCP + chloramphenicol). (e) Effect of acute treatments on the BR-body diameter, which is estimated as the maximum span of the cluster identified using density-based cluster analysis following each treatment. Horizontal lines indicate the mean of the distribution of exponential phase and stationary phase BR-body diameters. Number of clusters analyzed: 20 per condition. (f) Changes in the density of RNE-mEos3.2 single-molecule localizations within BR-bodies following each treatment. Horizontal lines indicate the mean of the distribution of exponential phase and stationary phase BR-body densities. Number of clusters analyzed: 20 per condition. (g) Dynamics inside BR-bodies in cells during prolonged stationary phase. Representative fluorescence recovery after photobleaching (FRAP) experiment kymographs during early (6 h) and late (24 h) stationary phase cells showing the bleaching and recovery of the RNE-mEos3.2 foci (blue) as a function of time, *t*. Scale bar: 500 nm. (h) FRAP of RNE-mEos3.2 in cells at the early and late stationary phase. $N$ = 20 foci. Error bars in a and c: standard deviation from three biological replicates. Statistics in a, e, and f: *** denotes $p < 0.001$, ** denotes $p < 0.005$, and n.s. denotes $p > 0.05$.

174 phase (Fig. 1d). However, when cells are treated with the combination of CCCP and
175 chloramphenicol, BR-bodies remain short-lived, similar to those observed during exponential phase
176 in the absence of stress (Fig. 2b). Similarly, BR-bodies remain short-lived when cells are treated with
177 chloramphenicol only (Supplementary Figure 3). This finding suggests that the increased lifespan of
178 BR-bodies upon treatment with CCCP might be an indirect effect of dropping ATP levels inhibiting
179 translation rather than directly related to ATP availability. Translation is typically the most energy-
180 intensive process during exponential growth,[57,58] and ATP and GTP are essential for several steps in
181 translation, including the esterification of amino acids to tRNAs, selection of the aa-tRNAs to the
182 ribosome, the assembly of ribosomal subunits, and the translocation of ribosomes along the mRNA.
183 When NTP levels are decreased, these processes slow, resulting in reduced translation rates.
184 Additionally, biorthogonal non-canonical amino acid tagging (BONCAT) revealed a significant
185 decrease in translation levels during the late stationary phase, with reductions of 30-fold, as well as
186 in cells treated with puromycin, CCCP, and the combination of CCCP and chloramphenicol, all
187 relative to exponential phase (Fig. 2c, Extended Data Fig. 3).

188 Similar to the extended lifespan of BR-bodies observed upon treatment with CCCP and
189 puromycin, these treatments also replicated stationary-phase decreases in RNE-mEos3.2 diffusivity
190 inside the BR-bodies (Fig. 2d, Supplementary Figure 4a), BR-body size (Fig. 2e, Supplementary Figure
191 4b), RNE molecular density (Fig. 2f, Supplementary Figure 4c), and residence time within BR-bodies
192 (Extended Data Fig. 2). Conversely, cells treated with a combination of CCCP and chloramphenicol
193 do not rigidify. This finding suggests that the rigid material state transition in stationary phase requires
194 increased amounts of ribosome-free mRNA transcripts in the cytoplasm, whereas ATP scarcity alone
195 is insufficient.

196 We identified low ribosome occupancy as a key factor contributing to the rigid material state
197 of BR-bodies during stationary phase. However, under prolonged stress, biomolecular condensates

198 have been observed to mature from having liquid-like to solid-like properties.[1,59–63] Initially, their
199 components interact transiently: molecules freely rearrange and exchange with the surrounding
200 phase, resembling liquid behavior. Over time, mechanisms such as entanglement of disordered
201 polypeptides,[64] vitrification,[65] percolation,[66] and nucleation and elongation of amyloid-like fibers[67]
202 contribute to rigidification and decreased molecular dynamics.[68] We investigated the role of
203 maturation in BR-body rigidification by *in vivo* fluorescence recovery after photobleaching (FRAP) of
204 BR-bodies (RNE-mEos3.2) in cultures of *C. crescentus* cells at 6 hrs and 24 hrs into stationary phase
205 (Fig. 2g,h). The condensates become less dynamic over time in stationary phase. The BR-body
206 fluorescence recovers only minimally at both time points, consistent with a rigid material state, but
207 BR-bodies are slightly more dynamic at 6 hrs than at 24 hrs. To further investigate the role of
208 maturation, we reconstituted the system *in vitro* and extracted meaningful information based on
209 RNE, the first bacterial protein found to undergo LLPS at physiological concentrations without
210 crowding agents.[11] FRAP performed on RNE droplets reconstituted *in vitro* and aged with RNA for 30
211 min, 4 hrs, and 8 hrs (Extended Data Fig. 4) revealed that condensates aged for 30 min were
212 significantly more dynamic, with nearly full fluorescence recovery within 2.5 min, whereas
213 condensates aged for 4 hrs exhibited minimal recovery and 8 hrs were even less dynamic. These
214 results support the role of maturation in changing the material state of BR-bodies.

215 **The material state transition of BR-bodies during stress shifts their function from promoting**
216 **mRNA decay to facilitating mRNA storage**

217 Our *in vivo* and *in vitro* results establish that, during stress conditions, the internal dynamics
218 and structure of BR-bodies become more rigid. Previous two-color images of mRNA and RNE using
219 MS2 RNA labeling[69] and fluorescence *in situ* hybridization (FISH) during exponential growth have
220 shown that transcripts such as *rsaA* exhibit low colocalization (~28%) with RNE in BR-bodies in
221 conditions allowing active RNA degradation.[35] However, colocalization increases significantly (~80%)

222 when RNE endonuclease cleavage is blocked using an RNE active site mutation (ASM) involving the
223 two residues coordinating the catalytic $Mg^{2+}$ ion in the active site[35], which, taken together, suggests
224 mRNA decay within BR-bodies during exponential growth. These results suggest that the transition
225 to a more rigid material state, along with its associated effects, may enable BR-bodies to store mRNA
226 during stress conditions.

227 To investigate the role of BR-bodies in mRNA storage, we performed two-color imaging of RNE
228 and mRNA using a live-cell MS2 system and FISH, and we measured mRNA degradation rates using
229 quantitative reverse transcription polymerase chain reaction (qRT-PCR). Notably, this study employs
230 an MS2 system optimized to accurately track short-lived mRNAs.[70] We selected four key mRNA
231 transcripts needed for *C. crescentus* exponential growth: *rsaA*, *rne*, *spmX*, and *ctrA*. All four mRNAs
232 were previously found to be stabilized in an RNE-IDR truncation mutant incapable of making BR-
233 bodies, suggesting BR-bodies play a role in their degradation.[35,71] The RsaA S-layer protein is the most
234 abundant protein in *C. crescentus*[72]. RsaA was chosen for comparison with the prior result, where
235 RNE cleavage is blocked using the ASM, providing insight into the role of the catalytic activity of RNE
236 in the condensate and its effect on transcript recruitment into BR-bodies.[35] RNE is crucial in RNA
237 processing, degradation,[22,23] BR-body formation, and cell fitness.[11] The integral membrane protein
238 SpmX enables cell division by localizing the histidine kinase DivJ to the stalked pole.[73,74] Finally, CtrA
239 is a master regulator of the cell cycle; it controls chromosome replication and transcription, and it
240 modulates the expression of about 25% of cell cycle-regulated genes in *C. crescentus*.[75–79] These
241 strategically selected transcripts enabled us to thoroughly assess the role of BR-bodies in mRNA
242 storage under stress and to determine the relevance of the stored transcripts.

243 Images of MS2-labeled *ctrA*, *spmX*, and *rsaA* transcripts (Fig. 3a,b, and Extended Data Fig. 5)
244 highlight their higher recruitment to BR-bodies during stationary phase compared to exponential
245 phase; these data sets were quantified using Pearson correlation coefficients (PCC). All transcripts

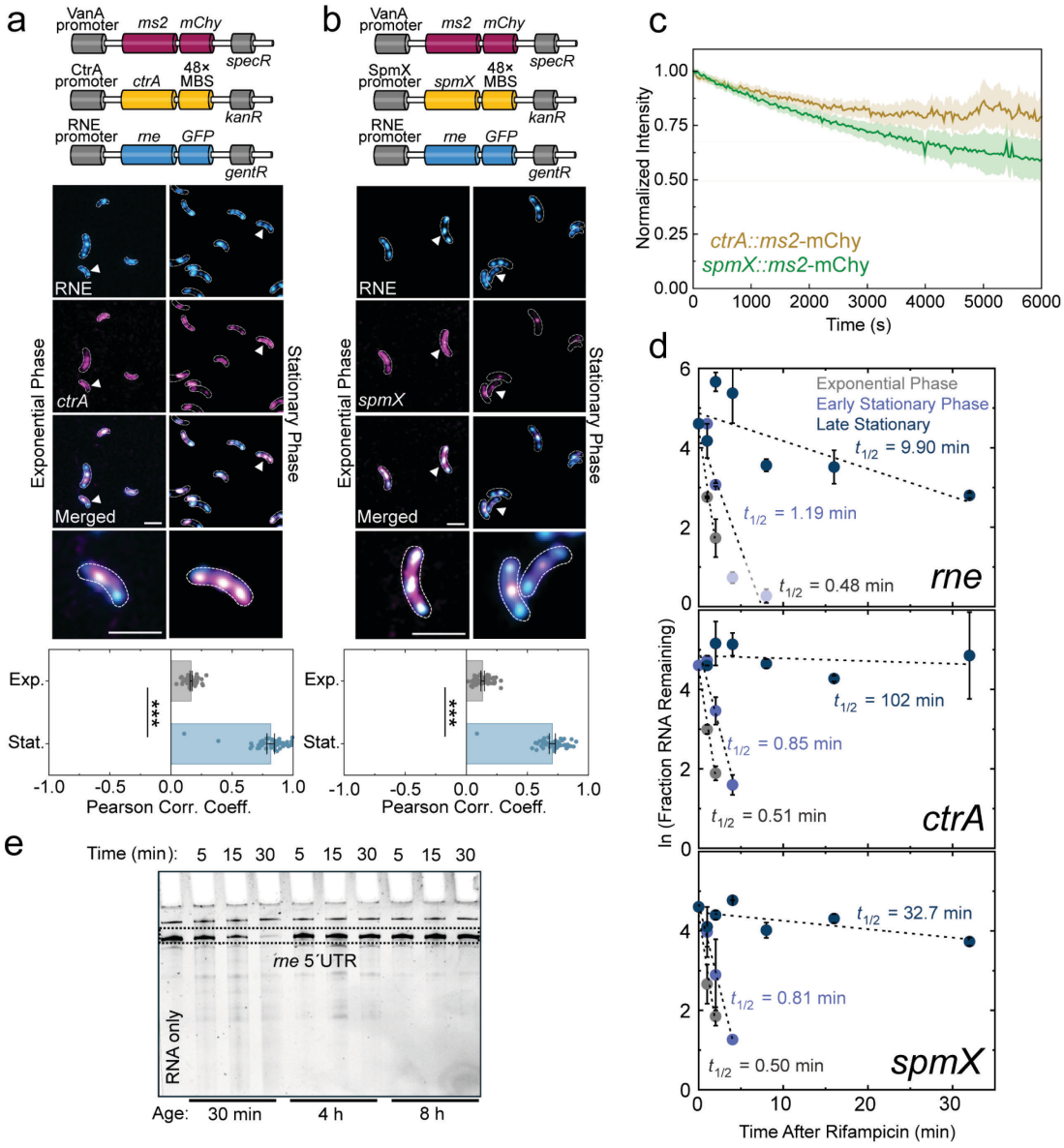


**Fig. 3 | Rigidification of BR-bodies switches their function from mRNA decay to storage of key growth mRNAs.**

**Fig. 3 | Rigidification of BR-bodies switches their function from mRNA decay to storage of key growth mRNAs.** (a,b) Stability of the *ctrA* (a) and *spmX* (b) transcripts in BR-bodies. Top: genetic constructs used to observe the transcript stability within the BR-bodies *in vivo*. Middle: Representative two-color images showing higher recruitment of the *ctrA* and *spmX* transcripts (magenta) to BR-bodies (blue) during stationary phase (left) relative to exponential phase (right). The merged channel is shown on two magnification levels for clarity. Bottom: Differences in recruitment quantified by the Pearson correlation coefficients between channels. Circles: PCC values for each cell. Error bars: SEM from 50 cells analyzed per phase. *** denotes $p < 0.001$. Arrowheads indicate representative foci. Scale bars in (a) and (b): 2 μm. (c) Decay profiles of *ctrA* and *spmX* in the late stationary growth phase. Analyses include $N = 108$ and 174 foci for the *ctrA* and *spmX* transcripts, respectively, measured across 28 and 49 cells, respectively. (d) qRT-PCR measurements of RNA half-lives for *rne*, *ctrA*, and *spmX* transcripts highlight the changes in transcript stability from exponential phase to the late stationary phase. Error bars: standard deviation from three biological replicates. (e) Condensate aging leads to decreased RNE cutting activity *in vitro*, as evidenced by the *rne* mRNA band in a 7% urea TBE/PAGE gel.

246 colocalize more with BR-bodies during stationary phase, similar to the behavior of *rsaA* when RNE
247 cleavage is blocked, suggesting significantly lower degradation activity by RNE during this phase. This
248 mRNA RNE colocalization is further confirmed by FISH (Supplementary Figure 5). To ensure that the
249 observed differences in BR-body colocalization across growth phases reflect transcript-specific
250 recruitment dynamics rather than analytical artifacts or changes in overall transcript abundance, we
251 used transfer-messenger mRNA (tmRNA) as a negative control. tmRNA is abundant in *C. crescentus,*
252 and is strongly depleted from the BR-bodies with a $\log_2$ fold-change of −2.8.[35] Upon applying the
253 same colocalization analysis to the target transcripts, we found that tmRNA colocalizes significantly
254 less with BR-bodies (PCC = 0.13 ± 0.04) compared to all other transcripts, even during exponential
255 phase (Supplementary Figure 6). These results confirm that the high levels of colocalization observed
256 for specific transcripts during stationary phase are not simply due to increased transcript
257 abundance; rather, they reflect selective recruitment into BR-bodies under stress.

258 We also assessed the stability of these transcripts tagged with MS2-RNA hairpins by
259 analyzing the photobleaching-corrected intensities of MS2-mChy foci colocalized with RNE foci
260 during both growth phases (Fig. 3c and Extended Data Fig. 5). To ensure that our observations
261 accurately reflect transcript stabilization and not artifacts of the labeling system, we employed two
262 versions of the MS2 system which are both utilized with a MS2-mChy dimerization deficient variant:[80]
263 a 48×-array with weaker MS2 coat protein RNA hairpin affinity[70] and a 96×-array.[35] Previous studies
264 have demonstrated that binding of the coat protein to MS2 binding sites artifactually stabilizes
265 mRNA.[81–83] Therefore, we confirmed that any observed accumulation of the mChy signal within BR-
266 bodies was due to real transcript stabilization and not an effect of the labeling system. As shown in
267 Fig. 3a,b, mChy foci do not colocalize with BR-bodies during exponential phase when using the 48×-
268 array system. However, using the 96×-array version (Extended Data Fig. 5), we observed mChy foci
269 colocalizing with BR-bodies, even during exponential phase. Despite the potential transcript

270 stabilization caused by the more perturbing 96×-array MS2 system, we still observed significant
271 differences in the decay profiles between exponential and stationary phases. During exponential
272 phase, MS2-mChy (96×-array) foci disassemble in under a few min, consistent with rapid internal
273 decay of mRNAs (Extended Data Fig. 5). In contrast, during stationary phase, MS2-mChy (48×-array)
274 foci and stably colocalize with BR-bodies for significantly longer, indicating slowed mRNA decay (Fig.
275 3c and Extended Data Fig. 5). To investigate the observations of the MS2-tagged RNAs, we measured
276 the RNA decay rates. mRNA half-life measurements by qRT-PCR confirmed this stabilization: *rne*,
277 *spmX*, and *ctrA* exhibit 20-, 65-, and 200-fold stability increases, respectively, from exponential to
278 late stationary phase (Fig. 3d), and the stabilization was confirmed by a second method, mRNA FISH,
279 for *ctrA* mRNA and *spmX* mRNA (Supplementary Figure 7). To test whether stabilization in stationary
280 phase depends on BR-body formation, we measured the stability of *spmX* and *ctrA* transcripts in
281 stationary phase cultures of *C. crescentus* expressing RNE-ΔCTD; these cells cannot assemble BR-
282 bodies.[11] In this background, transcript stabilization was reduced to only ~3-fold, confirming that BR-
283 bodies are essential for the pronounced stabilization of mRNA during stress (Supplementary Figure
284 7). Together, these measurements suggest that the rigid state of RNE is associated with a dramatic
285 slowdown in mRNA decay activity, consistent with a model in which BR-body material state regulates
286 RNA turnover.

287 Hfq is a well-known regulator of RNA stability, and in *E. coli*, Hfq was observed to form
288 condensates with RNA under conditions of nutrient deprivation, where it was also observed to
289 colocalize with *E. coli* RNE.[16,84,85] In *C. crescentus*, Hfq was observed to colocalize to a subpopulation
290 of BR-bodies,[43] suggesting it might impact the stability of transcripts in rigid BR-bodies observed in
291 stationary phase. To test whether the RNA chaperone Hfq, a BR-body constituent,[43] contributes to
292 transcript stabilization, we measured *ctrA* mRNA decay in a *Δhfq* background. In exponentially
293 growing *Δhfq* cells, *ctrA* mRNA decays slightly more slowly than in wild-type cells, but still degrades

294 rapidly (Supplementary Table 1), indicating that Hfq is not required for rapid turnover in exponential
295 phase. In stationary phase, *ctrA* mRNA remains highly stable in *Δhfq* cells, similarly to wild type,
296 suggesting that Hfq is not required for BR-body-mediated transcript stabilization. Consistently, the
297 diffusion profile of RNE-mEos3.2 within BR-bodies remains unchanged in the *Δhfq* background
298 (Supplementary Figure 8), indicating that the change to the rigid material state does not depend on
299 Hfq. Hence, the stabilization during stationary phase is independent of Hfq and instead reflects
300 protection conferred by the BR-body environment itself. As an additional control, we measured the
301 stability of tmRNA (Supplementary Table 1), a highly abundant transcript that is not enriched in the
302 BR-bodies. tmRNA remained fully stable in both exponential and stationary phases (> 8 min and > 16
303 min half-lives, respectively), confirming that transcripts not recruited into BR-bodies do not exhibit
304 phase-dependent changes in decay rate. This finding further supports the model that BR-body-
305 mediated stabilization depends on selective mRNA recruitment.

306 To investigate whether the reduced RNA cleavage activity of RNE is a direct result of
307 rigidification, we assessed the cutting activity of RNE in 30-min, 4-hr, and 8-hr *in vitro*-reconstituted
308 condensates (Fig. 3e). These aged RNE droplets were formed with RNE and RNA, but without $Mg^{2+}$,
309 an essential cofactor for RNA cleavage by RNE. At each droplet age, RNA cleavage was initiated by
310 adding $Mg^{2+}$, and samples were collected at various time points to assay RNA cleavage.[71] RNE
311 efficiently cleaves the *rne* 5' UTR in droplets aged for only 30 min,[71] with the corresponding band in
312 the PAGE gel disappearing within 30 min of $Mg^{2+}$ addition (Fig. 3e). In contrast, virtually no RNA
313 cleavage was observed in the rigidified droplets at the 4-hr and 8-hr timepoints. This finding suggests
314 that maturation into the rigid state can directly shut off RNE cleavage. Furthermore, we hypothesize
315 that BR-body formation during stress serves as a repository for mRNA and a means to sequester RNE
316 and potentially other degradative enzymes in an inactive state. This hypothesis is supported by the
317 higher amount of RNE in condensates during stationary phase, and by our recent work, where we

318 demonstrated that overexpression of RNA during exponential phase leads to growth arrest. Taken
319 together with our *in vitro* results, these results support a model in which BR-body rigidification
320 reduces RNE activity, allowing for selective preservation of mRNAs during stress.

321 **Fluidized BR-bodies are capable of the functional release of mRNAs**

322 Stored mRNAs may be useful for growth-arrested cells either by acting as a nutrient source
323 to promote regrowth or by being released to ribosomes to restart the translation program upon the
324 addition of new nutrients. To determine if mRNA release and subsequent translation can occur after
325 cells exit stationary phase and enter exponential growth, we assessed whether rigidification is
326 reversible by observing if stationary-state BR-bodies fluidize over time after nutrient replenishment
327 (Extended Data Fig. 6). Indeed, BR-body disassembly was detected after 90 min of nutrient
328 replenishment. We further investigated transcript storage by BR-bodies post-nutrient replenishment
329 by monitoring the colocalization of the *spmX* transcript with BR-bodies in stationary phase cultures
330 (Supplementary Figure 9). After 3 hrs, the colocalization profile of *spmX* with BR-bodies returns to
331 that observed during exponential phase (i.e., PCC = 0.22 ± 0.05 vs. 0.25 ± 0.04 in Fig. 3b), suggesting
332 that stored mRNA exits BR-bodies upon removal of stress.

333 Additionally, to evaluate whether these transcripts could be translated after exiting BR-
334 bodies, we performed a series of experiments designed to distinguish between translation of pre-
335 existing transcripts and translation of newly transcribed mRNAs. In wild-type *C. crescentus*, nutrient
336 replenishment after stationary phase was examined under conditions where new RNA synthesis was
337 blocked with rifampicin. RNE-mEos3.2 fluorescence recovered substantially over 6 hours following
338 whole-cell bleaching (Fig. 4a,b), indicating that recovery does not require transcription of new
339 mRNAs and must arise from mRNAs that existed prior to rifampicin treatment. To confirm that this
340 recovery reflects active translation rather than delayed protein maturation, we inhibited translation

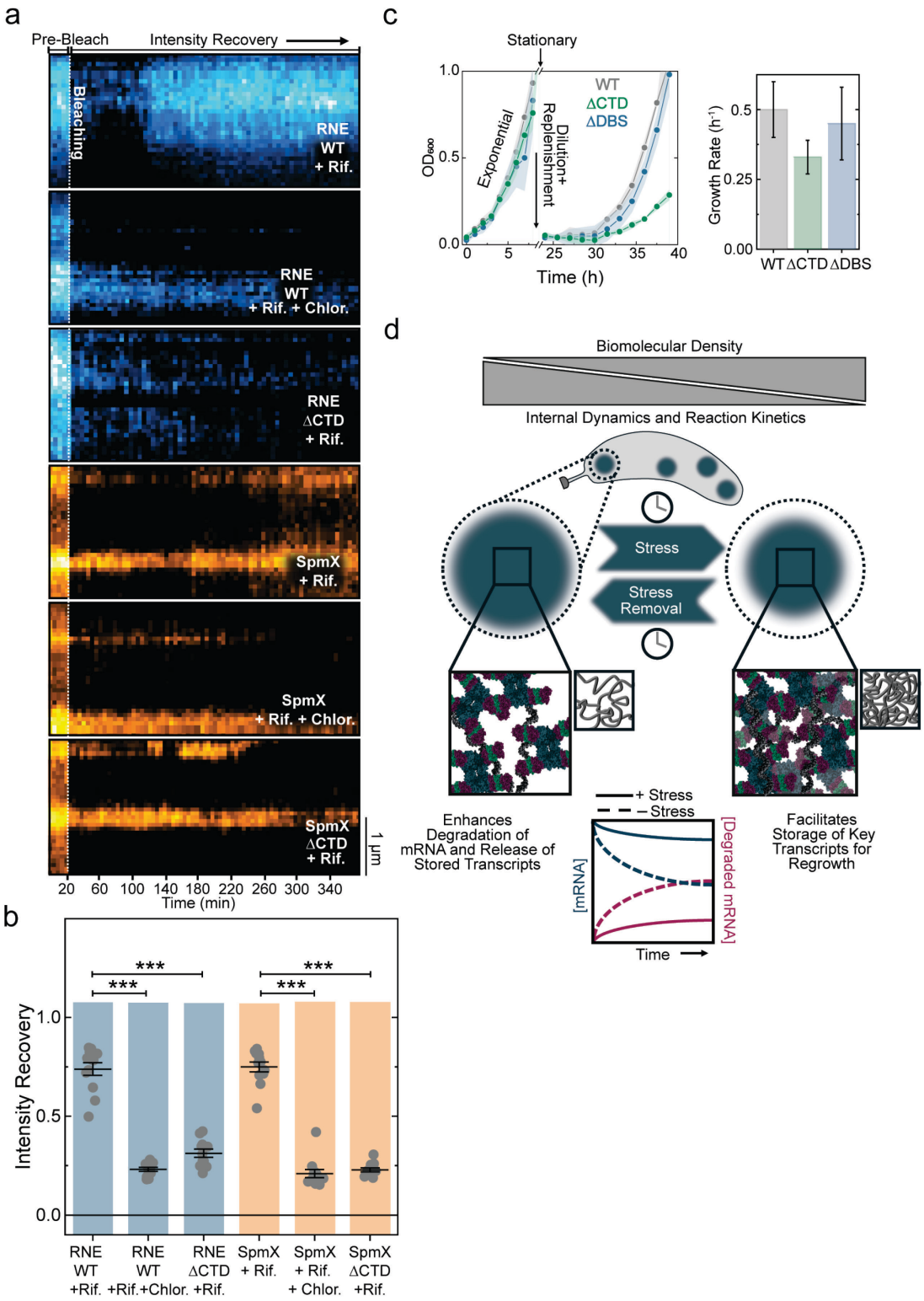


**Fig. 4 | Stored mRNAs can be translated and promote rapid growth.**

**Fig. 4 | Stored mRNAs can be translated and promote rapid growth.** (a) Representative kymographs of SpmX-mEos3.2 in both wild-type RNE and ΔCTD-RNE backgrounds, and of wild-type RNE and RNE-ΔCTD-mEos3.2 alone. Kymographs were generated by measuring cell fluorescence intensity along the long axis of stationary-phase *C. crescentus* cells after nutrient replenishment and inhibition of new transcript synthesis and translation with rifampicin and chloramphenicol, respectively. (b) Quantification of the recovery of the integrated intensity over the whole cell area at $t$ = 6 h relative to $t$ = 0 h following photobleaching of the whole cell intensity. Each dot below the distribution corresponds to the recovered intensity in one cell ($n$ = 12 cells), and the error bars indicate the standard error. *** denotes $p < 0.001$. (c) Functional implications of mRNA storage in BR-bodies. Left: comparison of the growth rate of *C. crescentus* cells with wild-type RNE vs. cells with RNE-ΔCTD (incapable of forming BR-bodies) or RNE-ΔDBS (forms BR-bodies but cannot assemble the degradosome) when cultures are back-diluted into PYE medium after 24 h in stationary phase. Right: growth rates following nutrient replenishment; error bars indicate the standard error. Cells expressing RNE-ΔCTD grow more slowly following nutrient replenishment, whereas cells expressing RNE-ΔDBS grow at rates comparable to wild-type. The initial growth curves, prior to entry into stationary phase, were initiated from back-dilutions of exponentially growing cultures. Three biological replicates were used for each condition. (d) Proposed model for how the material state of BR-bodies tunes their activity, enabling a transition from mRNA decay enhancement during growth to storage during stress.

341 with chloramphenicol, which abolished fluorescence recovery, indicating that the signal arises from
342 newly synthesized protein and not from maturation of pre-existing fluorescent proteins.

343 We then asked whether BR-bodies are required for this post-stress recovery. In cells
344 expressing RNE-ΔCTD, which are unable to form BR-bodies, fluorescence recovery for SpmX-
345 mEos3.2 and RNE-ΔCTD-mEos3.2 was minimal following nutrient replenishment and was similar to
346 the translation-inhibited wild-type cells (Fig. 4a,b). This result indicates that BR-bodies are required
347 to maintain mRNAs in a translatable state during stationary phase. Importantly, we observed a
348 similar behavior for *spmX* and *rne* transcripts, suggesting that BR-body-mediated transcript storage
349 and translation upon release is a general mechanism not limited to *rne*. To confirm the presence of
350 full-length mRNA that is capable of being translated within stationary phase BR-bodies, we amplified
351 the full-length *ctrA* mRNA by RT-PCR and found that full-length mRNA is indeed present within the
352 BR-body (Extended Data Fig. 5c). The observed translation of released mRNA from BR-bodies
353 suggests that BR-bodies can store functionally intact mRNAs for later translation upon stress
354 removal.

355 We ultimately assessed the functional implications of stress-induced mRNA storage in BR-
356 bodies by comparing the growth rate of *C. crescentus* cells with wild-type RNE to cells with RNE-
357 ΔCTD after 24 hrs in stationary phase (Fig. 4c). Remarkably, cells with RNE-ΔCTD exhibit a 1.5-fold
358 reduction in growth rate and a lag phase that is 3 hrs longer compared to the wild-type strain following
359 nutrient replenishment. To distinguish the role of BR-body formation from potential pleiotropic
360 effects of disrupting degradosome assembly, we analyzed recovery dynamics in an RNE-ΔDBS strain,
361 which lacks the degradosome binding sites on RNE and therefore cannot assemble the RNA
362 degradosome, but still forms condensates.[11] Upon nutrient replenishment, RNE-ΔDBS cells recover
363 with kinetics comparable to wild-type, in contrast to the slow recovery observed in the RNE-ΔCTD
364 strain (Fig. 4b,c). These results indicate that degradosome assembly is not required for the efficient

365 exit from stationary phase, and instead support the conclusion that the formation of BR-bodies and
366 their ability to store essential transcripts during stress play a critical role in enabling recovery. Thus,
367 this functional separation-of-function mutant demonstrates that the loss of condensate formation,
368 rather than general defects in RNA metabolism, compromises recovery in the RNE-ΔCTD mutant.

369 Altogether, these results suggest that during stress, BR-bodies play a critical role in storing
370 essential transcripts, which are then readily available for translation upon return to nutrient-repleted
371 conditions, contributing to a faster transition into exponential growth. This storage mechanism
372 circumvents the need to synthesize new transcripts, thereby facilitating the rapid program of protein
373 production necessary for regrowth. Importantly, we observed in *Agrobacterium tumefaciens* and
374 *Sinorhizobium meliloti* liquid-like BR-bodies also rigidify in stationary phase (Extended Data Fig. 7),
375 suggesting that the material state transition to mRNA storage may be a general feature of BR-bodies.

376 **Discussion**

377 BR-bodies are multifunctional biomolecular condensates that orchestrate RNA decay and
378 store RNA transcripts during stress (Fig. 4d). Under prolonged stress, BR-bodies rigidify, resulting in
379 decreased internal dynamics, higher biomolecular density, and compaction. This transition extends
380 the residence time of RNE within these condensates, reduces its degradation activity, and leads to
381 an altered degradosome deficient in RhlB. Consequently, RNA transcripts within BR-bodies are
382 stabilized under adverse conditions. Although a significant portion of RNE and mRNAs are
383 distributed outside BR-bodies, our data indicate that BR-body-localized RNE plays the dominant role
384 in transcript stabilization during stationary phase.

385 The stabilization of mRNA within BR-bodies is a functional bacterial adaptation that allows
386 the preservation of valuable epigenetic information during exposure to a variety of different stressors.
387 Upon stress removal, environmental and cellular conditions shift, triggering the restoration of

388 dynamics and disassembly of BR-bodies. This change facilitates the release of stabilized transcripts
389 back into the cytoplasm, where they can be promptly translated to support recovery and growth. This
390 elegant mechanism, wherein bacteria dynamically modulate the physical and biochemical
391 properties of BR-bodies in response to environmental cues, leverages phase separation and enzyme
392 kinetics to exert temporal and spatial control over RNA degradation and utilization. This mechanism
393 underscores how bacteria use biomolecular condensates not just as active enzymatic reaction sites
394 but also as adaptive tools for managing genetic resources to ensure survival and adaptation in
395 fluctuating environments.

396 The bacterial aggresome is another subcellular organelle that has recently been reported to
397 store mRNA under arsenic stress in *E. coli*.[12,13,86,87] Our results indicate that, like aggresomes, BR-
398 bodies store mRNA transcripts during stress conditions. However, the putative mechanisms by
399 which aggresomes and BR-bodies stabilize mRNA differ significantly from one another. Aggresomes
400 have been proposed to protect mRNA by excluding ribonucleases, with protein surface charge
401 playing a crucial role.[86] Aggresomes are thought to assemble through protein aggregation, and
402 although protein chaperones are enriched within aggresome structures, the molecular trigger of their
403 phase separation has not been uncovered.[12] However, whether aggresomes in *E. coli* might exclude
404 RNE,[88–90] the major mRNA decay nuclease, has not yet been explored. In contrast, RNE is the central
405 scaffold necessary for BR-body formation,[11] and rather than RNE being excluded from mature BR-
406 bodies, the material properties of the BR-bodies shut off the RNase activity. Interestingly, *C.*
407 *crescentus* BR-bodies have been found to enrich the aggresome marker proteins HslU, DnaK, and
408 ClpB,[43] suggesting some functional similarity to aggresomes, yet aggresomes have a dark color in
409 phase-contrast microscopy, whereas no such dark aggregates have been observed in *C. crescentus*
410 at stationary phase nor following heat shock, antibiotic treatment, or other stresses.[11,35,91,92]

411 Despite the mechanistic data in the current study, it is still unclear how mRNA stored within
412 BR-bodies is protected from RNE cleavage when cells transition from stationary to exponential
413 phase. Potential models for future research include the possibility that *C. crescentus* possesses RNE
414 inhibitor proteins stored within BR-bodies, similar to *E. coli* RraA and RraB.[93,94] Another hypothesis is
415 that the RNE catalytic domain is completely denatured during rigidification and requires refolding by
416 protein chaperones to become active again during the transition back to exponential growth.

417 Overall, we have determined that the function of the BR-bodies as sites of mRNA storage or
418 decay is dictated by their material state. This model of BR-bodies underscores their role as versatile
419 biomolecular condensates and also demonstrates how biophysical properties influence the
420 biochemical function of condensates. The ability to modulate enzymatic activity through controlled
421 biophysical changes within these condensates reveals a novel paradigm of gene expression
422 regulation, which is pivotal for bacterial survival in fluctuating environments.

423 **Data Availability**

424 All data generated and analyzed during this study are included in this published article and its
425 Supplementary Information files. Raw source data is available upon request.

426 **Code Availability**

427 Data processing and analysis scripts for this study were written in MATLAB and Python. The code
428 generated for this study is available on Github. Image analysis scripts:
429 https://github.com/BiteenMatlab/bacterial_condensates; and SMALL-LABS algorithm package:
430 https://github.com/BiteenMatlab/SMALL-LABS.

431 **Acknowledgments**

432 The authors acknowledge the support of NIH grant R35GM124733 to J.M.S., NIH T32GM142519-03
433 to HY., and NIH grants R01GM143182 and R01GM144731 to J.S.B. The authors thank Dr. Anthony
434 Vecchiarelli for generously providing access to his wide-field fluorescence microscope. Thanks to Dr.
435 Tamara Hendrickson and the WSU Department of Chemistry for lab space and equipment after the
436 Schrader lab was destroyed in a fire.

437 The authors declare no competing interests.

438 **Author contributions**

439 L.A.O.-R. designed, performed, and analyzed experiments (all live-cell single-molecule and
440 ensemble fluorescence imaging, FRAP, FISH, growth curves, and ATP level measurements),
441 interpreted results, and wrote the manuscript. H.Y. designed, performed, and analyzed experiments
442 (strain construction, qRT-PCR, and BONCAT) and interpreted results. V.N., A.H., and YZ designed,
443 performed, and analyzed experiments (all *in vitro* reconstitution and *in vitro* FRAP experiments) and
444 interpreted results. C.A.A. analyzed experiments (developed a script to isolate trajectories inside the
445 condensates) and contributed to writing the revised manuscript. J.C. analyzed experiments (cluster
446 analysis). J.M.S. provided expertise in the design and construction of the strains, interpreted results,
447 and wrote the manuscript. J.S.B. provided expertise in the design of live-cell imaging experiments,
448 designed experiments, interpreted results, and wrote the manuscript.

**References**

449 1. Banani, S. F., Lee, H. O., Hyman, A. A. & Rosen, M. K. Biomolecular condensates: organizers of
450 cellular biochemistry. *Nat. Rev. Mol. Cell Biol.* **18,** 285–298 (2017).

2. Boeynaems, S., Alberti, S., Fawzi, N. L., Mittag, T., Polymenidou, M., Rousseau, F., Schymkowitz, J., Shorter, J., Wolozin, B., Bosch, L. V. D., Tompa, P. & Fuxreiter, M. Protein Phase Separation: A New Phase in Cell Biology. *Trends Cell Biol.* **28,** 420–435 (2018).
3. Yoo, H., Triandafillou, C. & Drummond, D. A. Cellular sensing by phase separation: Using the process, not just the products. *J. Biol. Chem.* **294,** 7151–7159 (2019).
4. Ditlev, J. A., Case, L. B. & Rosen, M. K. Who's In and Who's Out—Compositional Control of Biomolecular Condensates. *J. Mol. Biol.* **430,** 4666–4684 (2018).
5. Nakamura, H., DeRose, R. & Inoue, T. Harnessing biomolecular condensates in living cells. *J. Biochem. (Tokyo)* **166,** 13–27 (2019).
6. Aguzzi, A. & Altmeyer, M. Phase Separation: Linking Cellular Compartmentalization to Disease. *Trends Cell Biol.* **26,** 547–558 (2016).
7. Ramaswami, M., Taylor, J. P. & Parker, R. Altered Ribostasis: RNA-Protein Granules in Degenerative Disorders. *Cell* **154,** 727–736 (2013).
8. Zhu, L., Richardson, T. M., Wacheul, L., Wei, M.-T., Feric, M., Whitney, G., Lafontaine, D. L. J. & Brangwynne, C. P. Controlling the material properties and rRNA processing function of the nucleolus using light. *Proc. Natl. Acad. Sci.* **116,** 17330–17335 (2019).
9. Dorone, Y., Boeynaems, S., Flores, E., Jin, B., Hateley, S., Bossi, F., Lazarus, E., Pennington, J. G., Michiels, E., Decker, M. D., Vints, K., Baatsen, P., Bassel, G. W., Otegui, M. S., Holehouse, A. S., Exposito-Alonso, M., Sukenik, S., Gitler, A. D. & Rhee, S. Y. A prion-like protein regulator of seed germination undergoes hydration-dependent phase separation. *Cell* **184,** 4284-4298.e27 (2021).
10. Bose, M., Lampe, M., Mahamid, J. & Ephrussi, A. Liquid-to-solid phase transition of *oskar* ribonucleoprotein granules is essential for their function in *Drosophila* embryonic development. *Cell* **185,** 1308-1324.e23 (2022).

475 11. Al-Husini, N., Tomares, D. T., Bitar, O., Childers, W. S. & Schrader, J. M. α-Proteobacterial RNA
476 Degradosomes Assemble Liquid-Liquid Phase-Separated RNP Bodies. *Mol. Cell* **71,** 1027-
477 1039.e14 (2018).
478 12. Pu, Y., Li, Y., Jin, X., Tian, T., Ma, Q., Zhao, Z., Lin, S., Chen, Z., Li, B., Yao, G., Leake, M. C., Lo, C.-
479 J. & Bai, F. ATP-Dependent Dynamic Protein Aggregation Regulates Bacterial Dormancy Depth
480 Critical for Antibiotic Tolerance. *Mol. Cell* **73,** 143-156.e4 (2019).
481 13. Jin, X., Lee, J.-E., Schaefer, C., Luo, X., Wollman, A. J. M., Payne-Dwyer, A. L., Tian, T., Zhang, X.,
482 Chen, X., Li, Y., McLeish, T. C. B., Leake, M. C. & Bai, F. Membraneless organelles formed by
483 liquid-liquid phase separation increase bacterial fitness. *Sci. Adv.* **7,** eabh2929 (2021).
484 14. Heinkel, F., Abraham, L., Ko, M., Chao, J., Bach, H., Hui, L. T., Li, H., Zhu, M., Ling, Y. M.,
485 Rogalski, J. C., Scurll, J., Bui, J. M., Mayor, T., Gold, M. R., Chou, K. C., Av-Gay, Y., McIntosh, L. P.
486 & Gsponer, J. Phase separation and clustering of an ABC transporter in Mycobacterium
487 tuberculosis. *Proc. Natl. Acad. Sci.* **116,** 16326–16331 (2019).
488 15. MacCready, J. S., Basalla, J. L. & Vecchiarelli, A. G. Origin and Evolution of Carboxysome
489 Positioning Systems in Cyanobacteria. *Mol. Biol. Evol.* **37,** 1434–1451 (2020).
490 16. McQuail, J., Carpousis, A. J. & Wigneshweraraj, S. The association between Hfq and RNase E in
491 long-term nitrogen-starved Escherichia coli. *Mol. Microbiol.* **117,** 54–66 (2022).
492 17. Azaldegui, C. A., Vecchiarelli, A. G. & Biteen, J. S. The emergence of phase separation as an
493 organizing principle in bacteria. *Biophys. J.* **120,** 1123–1138 (2021).
494 18. Saurabh, S., Chong, T. N., Bayas, C., Dahlberg, P. D., Cartwright, H. N., Moerner, W. E. &
495 Shapiro, L. ATP-responsive biomolecular condensates tune bacterial kinase signaling. *Sci. Adv.*
496 **8,** eabm6570 (2022).

497 19. Lasker, K., von Diezmann, L., Zhou, X., Ahrens, D. G., Mann, T. H., Moerner, W. E. & Shapiro, L.
498 Selective sequestration of signalling proteins in a membraneless organelle reinforces the
499 spatial regulation of asymmetry in Caulobacter crescentus. *Nat. Microbiol.* **5,** 418–429 (2020).
500 20. Surovtsev, I. V. & Jacobs-Wagner, C. Subcellular Organization: A Critical Feature of Bacterial
501 Cell Replication. *Cell* **172,** 1271–1293 (2018).
502 21. Treuner-Lange, A. & Søgaard-Andersen, L. Regulation of cell polarity in bacteria. *J. Cell Biol.*
503 **206,** 7–17 (2014).
504 22. Hammarlöf, D. L., Bergman, J. M., Garmendia, E. & Hughes, D. Turnover of mRNAs is one of the
505 essential functions of RNase E. *Mol. Microbiol.* **98,** 34–45 (2015).
506 23. Ono, M. & Kuwano, M. A conditional lethal mutation in an *Escherichia coli* strain with a longer
507 chemical lifetime of messenger RNA. *J. Mol. Biol.* **129,** 343–357 (1979).
508 24. Kedersha, N., Stoecklin, G., Ayodele, M., Yacono, P., Lykke-Andersen, J., Fritzler, M. J.,
509 Scheuner, D., Kaufman, R. J., Golan, D. E. & Anderson, P. Stress granules and processing bodies
510 are dynamically linked sites of mRNP remodeling. *J. Cell Biol.* **169,** 871–884 (2005).
511 25. Hubstenberger, A., Courel, M., Bénard, M., Souquere, S., Ernoult-Lange, M., Chouaib, R., Yi, Z.,
512 Morlot, J.-B., Munier, A., Fradet, M., Daunesse, M., Bertrand, E., Pierron, G., Mozziconacci, J.,
513 Kress, M. & Weil, D. P-Body Purification Reveals the Condensation of Repressed mRNA
514 Regulons. *Mol. Cell* **68,** 144-157.e5 (2017).
515 26. Youn, J.-Y., Dyakov, B. J. A., Zhang, J., Knight, J. D. R., Vernon, R. M., Forman-Kay, J. D. & Gingras,
516 A.-C. Properties of Stress Granule and P-Body Proteomes. *Mol. Cell* **76,** 286–294 (2019).
517 27. Rathnayaka-Mudiyanselage, I., Nandana, V. & Schrader, J. Proteomic composition of eukaryotic
518 and bacterial RNA decay condensates suggests convergent evolution. *Curr. Opin. Microbiol.*
519 **79,** 102467 (2024).

520 28. Brengues, M., Teixeira, D. & Parker, R. Movement of Eukaryotic mRNAs Between Polysomes and
521 Cytoplasmic Processing Bodies. *Science* **310,** 486–489 (2005).
522 29. Sheth, U. & Parker, R. Decapping and Decay of Messenger RNA Occur in Cytoplasmic
523 Processing Bodies. *Science* **300,** 805–808 (2003).
524 30. Xing, W., Muhlrad, D., Parker, R. & Rosen, M. K. A quantitative inventory of yeast P body proteins
525 reveals principles of composition and specificity. *eLife* **9,** e56525 (2020).
526 31. Blake, L. A., Watkins, L., Liu, Y., Inoue, T. & Wu, B. A rapid inducible RNA decay system reveals
527 fast mRNA decay in P-bodies. *Nat. Commun.* **15,** 2720 (2024).
528 32. Wheeler, J. R., Matheny, T., Jain, S., Abrisch, R. & Parker, R. Distinct stages in stress granule
529 assembly and disassembly. *eLife* **5,** e18413 (2016).
530 33. Moon, S. L., Morisaki, T., Khong, A., Lyon, K., Parker, R. & Stasevich, T. J. Multicolour single-
531 molecule tracking of mRNA interactions with RNP granules. *Nat. Cell Biol.* **21,** 162–168 (2019).
532 34. Mateju, D., Franzmann, T. M., Patel, A., Kopach, A., Boczek, E. E., Maharana, S., Lee, H. O.,
533 Carra, S., Hyman, A. A. & Alberti, S. An aberrant phase transition of stress granules triggered by
534 misfolded protein and prevented by chaperone function. *EMBO J.* **36,** 1669–1687 (2017).
535 35. Al-Husini, N., Tomares, D. T., Pfaffenberger, Z. J., Muthunayake, N. S., Samad, M. A., Zuo, T.,
536 Bitar, O., Aretakis, J. R., Bharmal, M.-H. M., Gega, A., Biteen, J. S., Childers, W. S. & Schrader, J.
537 M. BR-Bodies Provide Selectively Permeable Condensates that Stimulate mRNA Decay and
538 Prevent Release of Decay Intermediates. *Mol. Cell* **78,** 670-682.e8 (2020).
539 36. Chen, H., Shiroguchi, K., Ge, H. & Xie, X. S. Genome-wide study of mRNA degradation and
540 transcript elongation in Escherichia coli. *Mol. Syst. Biol.* **11,** 781 (2015).
541 37. Barnett, T. C., Bugrysheva, J. V. & Scott, J. R. Role of mRNA Stability in Growth Phase Regulation
542 of Gene Expression in the Group A Streptococcus. *J. Bacteriol.* **189,** 1866–1873 (2007).

543 38. Hambraeus, G., von Wachenfeldt, C. & Hederstedt, L. Genome-wide survey of mRNA half-lives
544 in Bacillus subtilis identifies extremely stable mRNAs. *Mol. Genet. Genomics* **269,** 706–714
545 (2003).
546 39. Dressaire, C., Pobre, V., Laguerre, S., Girbal, L., Arraiano, C. M. & Cocaign-Bousquet, M. PNPase
547 is involved in the coordination of mRNA degradation and expression in stationary phase cells of
548 Escherichia coli. *BMC Genomics* **19,** 848 (2018).
549 40. Esquerré, T., Laguerre, S., Turlan, C., Carpousis, A. J., Girbal, L. & Cocaign-Bousquet, M. Dual
550 role of transcription and transcript stability in the regulation of gene expression in Escherichia
551 coli cells cultured on glucose at different growth rates. *Nucleic Acids Res.* **42,** 2460–2472
552 (2014).
553 41. Morrison, J. M., Anderson, K. L., Beenken, K. E., Smeltzer, M. S. & Dunman, P. M. The
554 staphylococcal accessory regulator, SarA, is an RNA-binding protein that modulates the mRNA
555 turnover properties of late-exponential and stationary phase Staphylococcus aureus cells.
556 *Front. Cell. Infect. Microbiol.* **2,** (2012).
557 42. Zhang, M., Chang, H., Zhang, Y., Yu, J., Wu, L., Ji, W., Chen, J., Liu, B., Lu, J., Liu, Y., Zhang, J., Xu,
558 P. & Xu, T. Rational design of true monomeric and bright photoactivatable fluorescent proteins.
559 *Nat. Methods* **9,** 727–729 (2012).
560 43. Nandana, V., Rathnayaka-Mudiyanselage, I. W., Muthunayake, N. S., Hatami, A., Mousseau, C.
561 B., Ortiz-Rodríguez, L. A., Vaishnav, J., Collins, M., Gega, A., Mallikaarachchi, K. S., Yassine, H.,
562 Ghosh, A., Biteen, J. S., Zhu, Y., Champion, M. M., Childers, W. S. & Schrader, J. M. The BR-body
563 proteome contains a complex network of protein-protein and protein-RNA interactions. *Cell*
564 *Rep.* **42,** 113229 (2023).
565 44. Hardwick, S. W., Chan, V. S. Y., Broadhurst, R. W. & Luisi, B. F. An RNA degradosome assembly
566 in Caulobacter crescentus. *Nucleic Acids Res.* **39,** 1449–1459 (2011).

567 45. Ester, M., Kriegel, H.-P., Sander, J. & Xu, X. A density-based algorithm for discovering clusters in
568 large spatial databases with noise. in *Proc. Second Int. Conf. Knowl. Discov. Data Min*. 226–231
569 (AAAI Press, 1996).
570 46. Parry, B. R., Surovtsev, I. V., Cabeen, M. T., O'Hern, C. S., Dufresne, E. R. & Jacobs-Wagner, C.
571 The Bacterial Cytoplasm Has Glass-like Properties and Is Fluidized by Metabolic Activity. *Cell*
572 **156,** 183–194 (2014).
573 47. Kroschwald, S., Maharana, S., Mateju, D., Malinovska, L., Nüske, E., Poser, I., Richter, D. &
574 Alberti, S. Promiscuous interactions and protein disaggregases determine the material state of
575 stress-inducible RNP granules. *eLife* **4,** e06807 (2015).
576 48. Kroschwald, S., Maharana, S. & Simon, A. Hexanediol: a chemical probe to investigate the
577 material properties of membrane-less compartments. *Matters* (2017).
578 doi:10.19185/matters.201702000010
579 49. Lin, Y., Mori, E., Kato, M., Xiang, S., Wu, L., Kwon, I. & McKnight, S. L. Toxic PR Poly-Dipeptides
580 Encoded by the C9orf72 Repeat Expansion Target LC Domain Polymers. *Cell* **167,** 789-802.e12
581 (2016).
582 50. Hondele, M., Sachdev, R., Heinrich, S., Wang, J., Vallotton, P., Fontoura, B. M. A. & Weis, K.
583 DEAD-box ATPases are global regulators of phase-separated organelles. *Nature* **573,** 144–148
584 (2019).
585 51. Deng, Y., Beahm, D. R., Ionov, S. & Sarpeshkar, R. Measuring and modeling energy and power
586 consumption in living microbial cells with a synthetic ATP reporter. *BMC Biol.* **19,** 101 (2021).
587 52. Weber, S. C., Spakowitz, A. J. & Theriot, J. A. Nonthermal ATP-dependent fluctuations contribute
588 to the in vivo motion of chromosomal loci. *Proc. Natl. Acad. Sci.* **109,** 7338–7343 (2012).
589 53. Russell, R., Jarmoskaite, I. & Lambowitz, A. M. Toward a molecular understanding of RNA
590 remodeling by DEAD-box proteins. *RNA Biol.* **10,** 44–55 (2013).

591 54. Li, X.-Z., Plésiat, P. & Nikaido, H. The Challenge of Efflux-Mediated Antibiotic Resistance in
592 Gram-Negative Bacteria. *Clin. Microbiol. Rev.* **28,** 337–418 (2015).
593 55. Nathans, D. Puromycin inhibition of protein synthesis: incorporation of puromycin into peptide
594 chains. *Proc. Natl. Acad. Sci.* **51,** 585–592 (1964).
595 56. Oh, E., Becker, A. H., Sandikci, A., Huber, D., Chaba, R., Gloge, F., Nichols, R. J., Typas, A.,
596 Gross, C. A., Kramer, G., Weissman, J. S. & Bukau, B. Selective Ribosome Profiling Reveals the
597 Cotranslational Chaperone Action of Trigger Factor In Vivo. *Cell* **147,** 1295–1308 (2011).
598 57. Pontes, M. H., Sevostyanova, A. & Groisman, E. A. When Too Much ATP Is Bad for Protein
599 Synthesis. *J. Mol. Biol.* **427,** 2586–2594 (2015).
600 58. Stouthamer, A. H. A theoretical study on the amount of ATP required for synthesis of microbial
601 cell material. *Antonie Van Leeuwenhoek* **39,** 545–565 (1973).
602 59. Patel, A., Lee, H. O., Jawerth, L., Maharana, S., Jahnel, M., Hein, M. Y., Stoynov, S., Mahamid, J.,
603 Saha, S., Franzmann, T. M., Pozniakovski, A., Poser, I., Maghelli, N., Royer, L. A., Weigert, M.,
604 Myers, E. W., Grill, S., Drechsel, D., Hyman, A. A. & Alberti, S. A Liquid-to-Solid Phase Transition
605 of the ALS Protein FUS Accelerated by Disease Mutation. *Cell* **162,** 1066–1077 (2015).
606 60. Molliex, A., Temirov, J., Lee, J., Coughlin, M., Kanagaraj, A. P., Kim, H. J., Mittag, T. & Taylor, J. P.
607 Phase Separation by Low Complexity Domains Promotes Stress Granule Assembly and Drives
608 Pathological Fibrillization. *Cell* **163,** 123–133 (2015).
609 61. Zhang, H., Elbaum-Garfinkle, S., Langdon, E. M., Taylor, N., Occhipinti, P., Bridges, A. A.,
610 Brangwynne, C. P. & Gladfelter, A. S. RNA Controls PolyQ Protein Phase Transitions. *Mol. Cell*
611 **60,** 220–230 (2015).
612 62. Lin, Y., Protter, D. S. W., Rosen, M. K. & Parker, R. Formation and Maturation of Phase-Separated
613 Liquid Droplets by RNA-Binding Proteins. *Mol. Cell* **60,** 208–219 (2015).

614 63. Xiang, S., Kato, M., Wu, L. C., Lin, Y., Ding, M., Zhang, Y., Yu, Y. & McKnight, S. L. The LC Domain
615 of hnRNPA2 Adopts Similar Conformations in Hydrogel Polymers, Liquid-like Droplets, and
616 Nuclei. *Cell* **163,** 829–839 (2015).
617 64. Watanabe, H. Viscoelasticity and dynamics of entangled polymers. *Prog. Polym. Sci.* **24,** 1253–
618 1403 (1999).
619 65. Halfmann, R. A glass menagerie of low complexity sequences. *Curr. Opin. Struct. Biol.* **38,** 18–
620 25 (2016).
621 66. Mittag, T. & Pappu, R. V. A conceptual framework for understanding phase separation and
622 addressing open questions and challenges. *Mol. Cell* **82,** 2201–2214 (2022).
623 67. Boke, E., Ruer, M., Wühr, M., Coughlin, M., Lemaitre, R., Gygi, S. P., Alberti, S., Drechsel, D.,
624 Hyman, A. A. & Mitchison, T. J. Amyloid-like Self-Assembly of a Cellular Compartment. *Cell*
625 **166,** 637–650 (2016).
626 68. Linsenmeier, M., Hondele, M., Grigolato, F., Secchi, E., Weis, K. & Arosio, P. Dynamic arrest and
627 aging of biomolecular condensates are modulated by low-complexity domains, RNA and
628 biochemical activity. *Nat. Commun.* **13,** 3030 (2022).
629 69. Bertrand, E., Chartrand, P., Schaefer, M., Shenoy, S. M., Singer, R. H. & Long, R. M. Localization
630 of ASH1 mRNA Particles in Living Yeast. *Mol. Cell* **2,** 437–445 (1998).
631 70. Tutucci, E., Vera, M., Biswas, J., Garcia, J., Parker, R. & Singer, R. H. An improved MS2 system for
632 accurate reporting of the mRNA life cycle. *Nat. Methods* **15,** 81–89 (2018).
633 71. Nandana, V., Al-Husini, N., Vaishnav, A., Dilrangi, K. H. & Schrader, J. M. Caulobacter
634 crescentus RNase E condensation contributes to autoregulation and fitness. *Mol. Biol. Cell* **35,**
635 ar104 (2024).
636 72. Awram, P. & Smit, J. The Caulobacter crescentus Paracrystalline S-Layer Protein Is Secreted by
637 an ABC Transporter (Type I) Secretion Apparatus. *J. Bacteriol.* **180,** 3062–3069 (1998).

638 73. Wheeler, R. T. & Shapiro, L. Differential Localization of Two Histidine Kinases Controlling
639 Bacterial Cell Differentiation. *Mol. Cell* **4,** 683–694 (1999).
640 74. Radhakrishnan, S. K., Thanbichler, M. & Viollier, P. H. The dynamic interplay between a cell fate
641 determinant and a lysozyme homolog drives the asymmetric division cycle of Caulobacter
642 crescentus. *Genes Dev.* **22,** 212–225
643 75. Ryan, K. R., Judd, E. M. & Shapiro, L. The CtrA Response Regulator Essential for *Caulobacter*
644 *crescentus* Cell-cycle Progression Requires a Bipartite Degradation Signal for Temporally
645 Controlled Proteolysis. *J. Mol. Biol.* **324,** 443–455 (2002).
646 76. Wortinger, M., Sackett, M. J. & Brun, Y. V. CtrA mediates a DNA replication checkpoint that
647 prevents cell division in Caulobacter crescentus. *EMBO J.* **19,** 4503–4512 (2000).
648 77. Laub, M. T., Chen, S. L., Shapiro, L. & McAdams, H. H. Genes directly controlled by CtrA, a
649 master regulator of the Caulobacter cell cycle. *Proc. Natl. Acad. Sci.* **99,** 4632–4637 (2002).
650 78. Laub, M. T., McAdams, H. H., Feldblyum, T., Fraser, C. M. & Shapiro, L. Global Analysis of the
651 Genetic Network Controlling a Bacterial Cell Cycle. *Science* **290,** 2144–2148 (2000).
652 79. Quon, K. C., Marczynski, G. T. & Shapiro, L. Cell Cycle Control by an Essential Bacterial Two-
653 Component Signal Transduction Protein. *Cell* **84,** 83–93 (1996).
654 80. LeCuyer, K. A., Behlen, L. S. & Uhlenbeck, O. C. Mutants of the Bacteriophage MS2 Coat Protein
655 That Alter Its Cooperative Binding to RNA. *Biochemistry* **34,** 10600–10606 (1995).
656 81. Garcia, J. F. & Parker, R. MS2 coat proteins bound to yeast mRNAs block 5' to 3' degradation and
657 trap mRNA decay products: implications for the localization of mRNAs by MS2-MCP system.
658 *RNA* **21,** 1393–1395 (2015).
659 82. Heinrich, S., Sidler, C. L., Azzalin, C. M. & Weis, K. Stem–loop RNA labeling can affect nuclear
660 and cytoplasmic mRNA processing. *RNA* **23,** 134–141 (2017).

661 83. Garcia, J. F. & Parker, R. Ubiquitous accumulation of 3' mRNA decay fragments in
662 Saccharomyces cerevisiae mRNAs with chromosomally integrated MS2 arrays. *RNA* **22,** 657
663 (2016).
664 84. Guan, J., Hurto, R. L., Rai, A., Azaldegui, C. A., Ortiz-Rodríguez, L. A., Biteen, J. S., Freddolino, L.
665 & Jakob, U. HP-Bodies – Ancestral Condensates that Regulate RNA Turnover and Protein
666 Translation in Bacteria. 2025.02.06.636932 Preprint at
667 https://doi.org/10.1101/2025.02.06.636932 (2025)
668 85. Goldberger, O., Szoke, T., Nussbaum-Shochat, A. & Amster-Choder, O. Heterotypic phase
669 separation of Hfq is linked to its roles as an RNA chaperone. *Cell Rep.* **41,** 111881 (2022).
670 86. Pei, L., Xian, Y., Yan, X., Schaefer, C., Syeda, A. H., Howard, J., Liao, H., Bai, F., Leake, M. C. &
671 Pu, Y. Bacterial stress granule protects mRNA through ribonucleases exclusion.
672 2024.04.27.591437 Preprint at https://doi.org/10.1101/2024.04.27.591437 (2024)
673 87. Bollen, C., Louwagie, S., Deroover, F., Duverger, W., Khodaparast, L., Khodaparast, L., Hofkens,
674 D., Schymkowitz, J., Rousseau, F., Dewachter, L. & Michiels, J. Composition and liquid-to-solid
675 maturation of protein aggregates contribute to bacterial dormancy development and recovery.
676 *Nat. Commun.* **16,** 1046 (2025).
677 88. Mudd, E. A., Krisch, H. M. & Higgins, C. F. RNase E, an endoribonuclease, has a general role in
678 the chemical decay of Escherichia coli mRNA: evidence that rne and ams are the same genetic
679 locus. *Mol. Microbiol.* **4,** 2127–2135 (1990).
680 89. Górna, M. W., Carpousis, A. J. & Luisi, B. F. From conformational chaos to robust regulation: the
681 structure and function of the multi-enzyme RNA degradosome. *Q. Rev. Biophys.* **45,** 105–145
682 (2012).
683 90. Bandyra, K. J., Bouvier, M., Carpousis, A. J. & Luisi, B. F. The social fabric of the RNA
684 degradosome. *Biochim. Biophys. Acta BBA - Gene Regul. Mech.* **1829,** 514–522 (2013).

685 91. Schramm, F. D., Schroeder, K., Alvelid, J., Testa, I. & Jonas, K. Growth-driven displacement of
686 protein aggregates along the cell length ensures partitioning to both daughter cells in
687 Caulobacter crescentus. *Mol. Microbiol.* **111,** 1430–1448 (2019).
688 92. Wortinger, M. A., Quardokus, E. M. & Brun, Y. V. Morphological adaptation and inhibition of cell
689 division during stationary phase in Caulobacter crescentus. *Mol. Microbiol.* **29,** 963–973 (1998).
690 93. Lee, K., Zhan, X., Gao, J., Qiu, J., Feng, Y., Meganathan, R., Cohen, S. N. & Georgiou, G. RraA: a
691 Protein Inhibitor of RNase E Activity that Globally Modulates RNA Abundance in E. coli. *Cell*
692 **114,** 623–634 (2003).
693 94. Górna, M. W., Pietras, Z., Tsai, Y.-C., Callaghan, A. J., Hernández, H., Robinson, C. V. & Luisi, B.
694 F. The regulatory protein RraA modulates RNA-binding and helicase activities of the E. coli RNA
695 degradosome. *RNA* **16,** 553–562 (2010).